NASA TECHNICAL MEMORANDUM

NASA TM X-3224

NASA TM X-3224

COLD-AIR ANNULAR-CASCADE INVESTIGATION OF AERODYNAMIC PERFORMANCE OF CORE-ENGINE-COOLED TURBINE VANES

I - Solid-Vane Performance and Facility Description

Louis J. Goldman and Kerry L. McLallin

Lewis Research Center

Cleveland, Ohio 44135

NATIONAL AERONAUTICS AND SPACE ADMINISTRATION • WASHINGTON, D. C. • APRIL 1975

1. Report No.	2. Government Accession No.	3. Recipient's Catalog No.
NASA TM X-3224		

4. Title and Subtitle	5. Report Date
COLD-AIR ANNULAR-CASCADE INVESTIGATION OF AERODYNAMIC PERFORMANCE OF CORE-ENGINE-COOLED TURBINE VANES. I - SOLID-VANE PERFORMANCE AND FACILITY DESCRIPTION	April 1975
	6. Performing Organization Code

7. Author(s)	8. Performing Organization Report No.
Louis J. Goldman and Kerry L. McLallin	E-8214
	10. Work Unit No. 505-04

9. Performing Organization Name and Address	11. Contract or Grant No.
Lewis Research Center National Aeronautics and Space Administration Cleveland, Ohio 44135	
	13. Type of Report and Period Covered Technical Memorandum
12. Sponsoring Agency Name and Address National Aeronautics and Space Administration Washington, D.C. 20546	14. Sponsoring Agency Code

15. Supplementary Notes

16. Abstract

The aerodynamic performance of a solid (uncooled) version of a core engine cooled stator vane was experimentally determined in a full-annular cascade, where three-dimensional effects could be obtained. The solid vane, which serves as a basis for comparison with subsequent cooled tests, was tested over a range of aftermixed critical velocity ratios of 0.57 to 0.90. Overall vane aftermixed efficiencies were obtained over this critical velocity ratio range and compared with results from a two-dimensional cascade. The variation in vane efficiency and aftermixed flow conditions with circumferential and radial position were obtained and compared with design values. Vane surface static-pressure distributions were also measured and compared with theoretical results.

17. Key Words (Suggested by Author(s))	18. Distribution Statement
Aerodynamic performance Annular cascade Cooled vanes Secondary flow	Unclassified - unlimited STAR Category 02 (rev.)

19. Security Classif. (of this report)	20. Security Classif. (of this page)	21. No. of Pages	22. Price*
Unclassified	Unclassified	24	$3.75

* For sale by the National Technical Information Service, Springfield, Virginia 22151

COLD-AIR ANNULAR-CASCADE INVESTIGATION OF AERODYNAMIC PERFORMANCE OF CORE-ENGINE-COOLED TURBINE VANES I - SOLID-VANE PERFORMANCE AND FACILITY DESCRIPTION

by Louis J. Goldman and Kerry L. McLallin

Lewis Research Center

SUMMARY

The aerodynamic performance of a solid (uncooled) version of a core engine cooled stator vane was experimentally determined in a full-annular cascade, where three-dimensional effects could be obtained. This vane was of the same size and profile as the cooled vanes to be subsequently tested and would serve as a basis of comparison for these tests. The solid vanes were tested over a pressure ratio range that corresponds to mean-radius ideal aftermixed critical velocity ratios of 0.57 to 0.90. The design value for the vane is 0.778. Vane surface static-pressure distributions were measured and corresponding critical velocity ratios were compared with theoretical results. The variation in vane efficiency and aftermixed flow conditions with circumferential and radial position were obtained and compared with design values. Overall vane aftermixed efficiencies were obtained over this critical velocity ratio range and compared with results obtained in a two-dimensional cascade.

It was found that the experimental vane surface critical velocity ratio distributions agreed well with the theoretical calculations. At the vane exit survey plane two vortex cores of high loss concentration were noted at the corners formed by the end walls and the suction surface of the vanes. These loss regions were associated with secondary flows in the annular cascade. In the vortex regions, the aftermixed flow angle was found to be underturned by about 2° to 4°.

The overall aftermixed efficiency and the aftermixed efficiency at the mean radius for design critical velocity ratio were 0.960 and 0.978, respectively, and varied only slightly with critical velocity ratio over the range investigated. The kinetic energy losses due to end wall boundary layers and secondary flow was experimentally determined to be 0.018 at the design critical velocity ratio. It was analytically determined that the end wall boundary layer loss was 0.007 and therefore the loss due to secondary flow was 0.011 for this vane.

INTRODUCTION

Research studies are being conducted at the NASA Lewis Research Center to investigate the performance of air-cooled blading for high-temperature core-engine turbines. As part of this effort, the performance of a solid (uncooled) core turbine (half scale) has been obtained and reported in reference 1. These results will form the basis for comparison with the cooled versions of the core turbine. The performance of the solid core turbine stator vanes (full size), tested in a two-dimensional cascade, has been reported in reference 2. These results, although indicative of the vane performance at the mean section, do not include end wall or secondary flow losses. Because of the relatively small-sized blading and the low aspect ratio (vane height to vane axial chord of one) both of these losses may be significant.

Consequently, an investigation was undertaken wherein the core-turbine stator vane (full size and same aerodynamic profile as refs. 1 and 2) would be studied in a full-annular cascade where three-dimensional effects could be obtained. The annular cascade was designed primarily for cold-air studies at a primary-to-coolant total temperature ratio of 1. The first phase of the study was to obtain the three-dimensional performance of the (uncooled) solid vane. Comparison with the two-dimensional cascade results would then indicate the significance of the end wall and the secondary flow losses. Subsequent studies would then determine the performance of different vane cooling schemes for comparison with the full-annular solid vane results.

The investigation of the solid vanes was conducted over a pressure ratio range that corresponded to mean-radius ideal aftermixed critical velocity ratios of 0.57 to 0.90. The design value for the vane at the mean section is 0.778. Annular surveys were made downstream of the vane trailing edge for this range of critical velocity ratios. Vane surface static-pressure measurements were obtained near design critical velocity ratio.

This report includes a description of the full-annular cascade facility and presents the experimental results for the solid vane. Vane surface critical velocity ratios corresponding to the surface static-pressure measurements are compared with theoretical results. The variation in vane efficiency and flow conditions with circumferential and radial position are presented. In addition, overall vane efficiencies were obtained and compared with the results from the two-dimensional cascade (ref. 2).

SYMBOLS

g force-mass conversion constant, 32.174 lbm-ft/lbf-sec^2

p pressure, N/m^2; lbf/ft^2

R gas constant, J/(kg)(K); ft-lbf/(lbm)($^\circ$R)

r	radial direction, m; ft
T	temperature, K; ^{o}R
V	velocity, m/sec; ft/sec
X	vane coordinates (fig. 3), cm; in.
Y	vane coordinates (fig. 3), cm; in.
α	flow angle measured from axial direction, rad; deg
γ	ratio of specific heats
η	local efficiency based on kinetic energy
$\overline{\eta}$	efficiency at radius r based on kinetic energy
$\overline{\overline{\eta}}$	overall efficiency based on kinetic energy
θ	circumferential direction, rad; deg
ρ	density, kg/m^3; lbm/ft^3

Subscripts:

cr	flow condition at Mach 1
i	survey position closest to inner (hub) wall
id	ideal or isentropic
L	lower surface
mean	mean radius
o	survey position closest to outer (tip) wall
s	vane surface
U	upper surface
z	axial direction
0	station at inlet plane of cascade bellmouth (fig. 2)
1	station at vane inlet (fig. 2)
2	station at vane trailing edge (fig. 2)
3	station downstream of vane trailing edge where survey measurements were taken (fig. 2)
3M	station downstream of vane trailing edge where flow is assumed to be circumferentially mixed (uniform) (fig. 2)

Superscript:

'	total-state condition

APPARATUS AND PROCEDURE

Cascade Facility

The full-annular cascade facility consists primarily of an inlet section, a test section, and an exit section. The actual facility and a cross-sectional view of the facility are shown in figures 1 and 2, respectively. In operation, atmospheric air is drawn through the inlet section, the blading, and the exit section and then exhausted through the laboratory altitude exhaust system.

Inlet section. - The inlet, consisting of a bellmouth and a short straight section, was designed to accelerate the flow to uniform axial flow at the vane inlet. The bellmouth profile was designed to provide a smooth transition to the straight section.

Test section. - The test section consists of a sector of five vanes which are part of the full-annular ring of 36 vanes. As seen in figure 2, the vanes pass through two hollow annular rings. This allows cooling air to be independently supplied to both the vanes and end walls. For the solid (uncooled) vane investigation reported herein, all 36 vanes were identical and no end wall cooling was employed. For subsequent cooling investigations, the same five-vane test sector will be employed.

The stator vane geometry (same aerodynamic profile as refs. 1 and 2) is shown in figure 3. The untwisted vanes, of constant profile from hub to tip, have a height of 3.81 centimeters (1.50 in.), an axial chord of 3.823 centimeters (1.505 in.), and a trailing edge radius of 0.089 centimeter (0.035 in.). The vane aspect ratio and the solidity at the mean section are 1.00 and 0.93, respectively (based on axial chord). The stator hub-to-tip radius ratio is 0.85 and the mean radius is 23.50 centimeters (9.25 in.). For completeness, the core turbine velocity diagram is shown in figure 4.

Exit section. - The exit section consists primarily of a diffusing section and a flow-straightening section. The diffusing section was designed to decelerate the flow gradually downstream of the test section. Because of mechanical failure, the diffuser was removed for this investigation (see fig. 2). This removal resulted in a more rapid deceleration of the flow but did not seem to affect cascade operation. The flow straightener was designed to turn the swirling flow back to the axial direction prior to its entering the laboratory exhaust system. The straightener consists of a bundle of short tubes with centerlines parallel to the cascade axis (fig. 2).

Instrumentation

Instrumentation was provided to measure wall static pressures at various locations, vane surface static pressures at different radii, and survey data of total pressure, static

pressure, and flow angle downstream of the test vanes. Figure 2 shows the station nomenclature used for the instrumentation.

Inlet total conditions. - Total temperature and pressure were measured at the cascade inlet (station 0). The total temperature of the entering room air was measured by four copper-constantan thermocouples located 90° apart circumferentially at the bellmouth inlet. The ambient total pressure was measured by a barometer.

Wall static pressures. - Static pressures were measured at various locations in the cascade by pressure taps located on both the inner (hub) and outer (tip) walls. At a distance of one axial-chord length upstream of the vane inlet (station 1), four taps were located 90° apart circumferentially. These static pressures were used to ascertain the uniformity of the flow entering the vanes as well as to provide information for estimating the incoming airflow rate. At the exit survey plane (station 3), 8 taps spanning the test vanes were located as shown in figure 5. These pressures were used to indicate the uniformity of the flow in the test section. Two static taps (inner and outer wall) were also located 10.2 centimeters (4.0 in.) downstream of the vanes where it was felt that the flow would be mixed to relatively uniform conditions (station 3M). The hub static pressure was used to set the flow conditions in the cascade.

Vane surface static pressures. - For the initial tests, two of the test vanes were instrumented with a total of 42 surface static-pressure taps as shown in figure 6. One vane was instrumented with 20 taps located at the mean radius. The second vane had 22 taps which were divided equally between sections located 0.51 centimeter (0.20 in.) from the vane hub and tip (fig. 6). As figure 6 shows, the pressure tubing was installed in grooves machined into the vane surface. After the tubing was installed, the grooves were filled and faired to the contour of the vane surface. The static-pressure taps were 0.051 centimeter (0.020 in.) in diameter and normal to the vane surface. Subsequent testing was performed by removing the two instrumented vanes and replacing them with noninstrumented solid vanes. This was done to ensure that the measured performance did not include any losses that might have been caused by the presence of the vane surface taps.

Survey probes. - Two different survey probes were used sequentially at the survey plane (station 3) to obtain the vane performance. A combination probe (fig. 7) was used initially for measurements away from the end walls. After completion of these measurements, the combination probe was removed and replaced with a two-element total pressure probe (fig. 8) for measurements near the walls. The survey plane (station 3) was located 1.3 centimeters (0.5 in.) downstream of the vane trailing edge in the axial direction. Both probes were positioned at a fixed angle of 67° from the axial direction, which corresponds to the design flow angle.

The calibrated combination probe measured total pressure, static pressure, and flow angle. The probe tip was made of stainless-steel tubing with an outside diameter of 0.067 centimeter (0.030 in.) and a wall thickness of 0.008 centimeter (0.003 in.).

The total pressure tube had an inside bevel of 30° (see fig. 5) which reduces the sensitivity of the measurement to flow angle (ref. 3). The loss in total pressure was measured using a differential pressure transducer referenced to atmospheric pressure. Static pressure was measured by using a Prandtl tube. The flow angle was determined from the measured pressure difference of two 45°-angled tubes (fig. 5) as described in reference 4. The survey area, which included the middle three of the five test vanes, is shown in figure 5.

For surveys near the end walls a two-element total pressure probe (fig. 8) was used. The probe tip was made of stainless-steel tubing with an outside diameter of 0.051 centimeter (0.020 in.) and an inside diameter of 0.038 centimeter (0.015 in.). The total pressure tubes again had an inside bevel of 30°. The upper element of the probe was used for measurements near the tip wall while the lower element was used near the hub wall.

Procedure

To operate the cascade facility, atmospheric air from the test cell was drawn through the cascade and exhausted into the laboratory altitude exhaust system. The test conditions were set by controlling the pressure ratio across the vane row with two throttle valves located in the exhaust system. The hub static tap located downstream of the test section, where the flow was assumed to be circumferentially uniform (station 3M), was used to set this pressure ratio.

The solid vanes were tested over a pressure ratio range that corresponded to mean-radius ideal aftermixed critical velocity ratios $(V_{3M}/V_{cr,\,3M})_{id,\,mean}$ of 0.57 to 0.90. The design value for the vane is 0.778. At a given pressure ratio, probe survey data were obtained at a number of different radii over the vane height. At any fixed radius, the probe was moved circumferentially over three vane passages with survey data being obtained continuously. The slow speed of the circumferential drive mechanism coupled with the data recording rate resulted in a cycle of survey data (i.e., probe position, total pressure, static pressure, and flow angle) being obtained at approximately 0.08° increments. The vane spacing in the annular cascade is 10°. The output signals of the calibrated pressure transducers were digitized and recorded on magnetic tape.

Data Reduction

The solid vane performance presented herein was calculated from the combination survey probe measurements of total pressure, static pressure, flow angle, and probe position. For the end wall survey probe where only total pressure was measured it was

necessary to estimate the static pressure and flow angle. The static pressure was assumed to vary linearly between the hub and tip wall values. Since the flow angle has no apparent effect on the calculated vane performance, a constant value of 67° was assumed. Data from the middle wake (of the three wakes that were measured) were used in these calculations.

The calculation of the vane efficiency is based on the determination of a hypothetical state where it is assumed that the flow has mixed to a circumferentially uniform condition (station 3M). At each radius, the conservation of mass, momentum, and energy is used to obtain this aftermixed state (i.e., $V_{3M,z}(r)$, $V_{3M}(r)$, $p_{3M}(r)$, $T_{3M}(r)$, $\alpha_{3M}(r)$, etc.) from the survey measurements. The calculation procedure is described more fully in reference 5. The aftermixed vane efficiency is used herein because it is theoretically independent of the axial location of the survey measurement plane. It should be noted that the aftermixed efficiency contains not only the vane profile loss but also the mixing loss.

For solid vanes, the vane aftermixed efficiency based on kinetic energy can be defined as a function of radius $\overline{\eta}_{3M}(r)$ or as an overall quantity $\overline{\overline{\eta}}_{3M}$, as given by the following equations from reference 5:

$$\overline{\eta}_{3M}(r) = \frac{V_{3M}^2(r)}{V_{3M,\,id}^2(r)} \tag{1}$$

$$\overline{\overline{\eta}}_{3M} = \frac{\int_{r_i}^{r_o} \rho_{3M}(r) V_{3M,z}(r) V_{3M}^2(r) r\, dr}{\int_{r_i}^{r_o} \rho_{3M}(r) V_{3M,z}(r) V_{3M,\,id}^2(r) r\, dr} \tag{2}$$

where

$$V_{3M,\,id}(r) = \sqrt{\left(\frac{2\gamma}{\gamma - 1}\right) g R T_o' \left\{1 - \left[\frac{p_{3M}(r)}{p_o'}\right]^{(\gamma-1)/\gamma}\right\}} \tag{3}$$

In the preceding equations, it has been assumed that the total pressure and temperature at the vane inlet (station 1) are equal to the total pressure and temperature at the cascade inlet (station 0).

RESULTS AND DISCUSSION

Vane Surface Critical Velocity Ratio Distributions

The vane surface critical velocity ratio distributions corresponding to the static pressures measured at the hub, mean, and tip radii are presented in figure 9. The surface distributions are compared with the theoretical results obtained from the computer programs CHANEL and TSONIC, described in references 6 and 7, respectively. CHANEL is a quasi-three-dimensional flow program but is limited to the guided portion of the vane passage. The TSONIC program calculates the flow conditions for the entire passage but is limited to two-dimensional flow. The variation of stream sheet thickness with axial position, which is needed as input for TSONIC, was obtained from the CHANEL results. Using the experimental exit conditions of weight flow, flow angle, and total pressure loss as input for TSONIC resulted in good agreement between the theoretical and experimental results. The CHANEL results are shown in figure 9 for comparison, and in general indicate more vane loading than either the experimental results or the TSONIC results. The differences in the theoretical results are due to the assumption made in CHANEL as to the variation of streamline curvature in the blade-to-blade direction. No such assumption is needed for TSONIC and therefore complete agreement between the two programs is not expected.

Survey Plane Flow Conditions and Vane Performance

The exit flow angle and critical velocity ratio at the survey plane (station 3) are shown in figure 10, for data obtained at the mean radius at an ideal aftermixed critical velocity ratio of 0.785. For comparison, the theoretical results obtained from TSONIC are also shown in the figure. The experimental and theoretical variation of exit flow angle are in good agreement. The critical velocities also agree well in the free-stream region. In the wake region, agreement was not expected since TSONIC is an inviscid solution. The experimental exit measurements are seen to be essentially periodic over the total survey travel.

A computer plot of efficiency contours is shown in figure 11 for a single vane passage tested at an ideal aftermixed critical velocity ratio of 0.785. The projection of the trailing edge to the survey plane, using the experimental flow angles, is also shown in the figure. Two cores of high loss (minimum efficiencies of about 0.72), centered at approximately 10 and 80 percent of the vane height, are located on the suction surface side of the trailing edge projection. These loss regions are associated with the secondary flows (ref. 8) which are formed when the boundary layers on the annulus walls are deflected through the vane passage (from pressure to suction surface of adjacent vanes).

This flow is then turned away from the end walls and rolls up to form passage vortexes in the corners formed by the end walls and the vane suction surface. The relatively large portion of the vane passage that is occupied by the vortex cores is typical of low aspect ratio vanes as seen, for example, by the results of reference 9.

Calculated Aftermixed Flow Conditions and Vane Performance

As discussed in the Data Reduction section, the aftermixed conditions, at each radius, are obtained from the survey measurements by application of the conservation of mass, momentum, and energy. The variation of aftermixed flow angle, $\alpha_{3M}(r)$ and aftermixed static-to-inlet total pressure ratio $p_{3M}(r)/p'_0$ with radial position, at an ideal aftermixed critical velocity ratio of 0.785, is shown in figure 12. The aftermixed flow angle is lower than the design value in the vortex core regions by about 2° to 4°. Near the tip wall the flow is overturned, which is consistent with the end wall crossflow from pressure to suction surface discussed previously. It is expected that similar results would have been obtained near the hub wall if flow angle measurements could have been obtained closer to the wall. The aftermixed static-to-inlet total pressure ratio varies almost linearly with radial position and agrees well with the design values.

The variation of aftermixed efficiency $\bar{\eta}_{3M}(r)$ with radial position at an ideal aftermixed critical velocity ratio of 0.785 is shown in figure 13. Results from both the combination and end wall total pressure probes are shown in the figure. Although the end wall total pressure probe was used primarily to obtain the losses near the walls, it was also used to take a complete radial survey over the vane height which shows excellent agreement with the results of the combination probe.

The higher losses of the vortex core regions are clearly noted in the figure. Minimum aftermixed efficiencies of 0.939 and 0.944 were obtained for the hub and tip vortices, respectively. A maximum efficiency of 0.978 was obtained at the mean radius. At the walls the efficiency drops off sharply because of the high losses associated with the end wall boundary layers.

The overall aftermixed efficiency $\bar{\bar{\eta}}_{3M}$ as a function of ideal aftermixed critical velocity ratio is shown in figure 14. For comparison, the two-dimensional cascade results (ref. 2) and the annular cascade results at the mean radius are also shown in the figure. These two efficiencies (which are indicative of the vane profile losses) are seen to be in good agreement except at the higher critical velocity ratios. Also shown, as a solid symbol, is the two-dimensional vane efficiency predicted analytically. Vane boundary-layer parameters were calculated assuming a turbulent boundary layer at the vane inlet using the computer program described in reference 10. Losses were then calculated by the method described by Stewart in reference 11. Reasonable agreement between theory and experiment was obtained. The overall aftermixed efficiency and the aftermixed

efficiency at the mean radius for design critical velocity ratio are 0.960 and 0.978, respectively, and vary only slightly with aftermixed critical velocity ratio. The difference in the mean radius and overall aftermixed efficiencies is 0.018 (i.e., 0.978 - 0.960) at design critical velocity ratio and is due to end wall and secondary flow losses. Secondary flow losses will be discussed in the next section.

Secondary Flow Losses

In the previous section, the kinetic energy loss due to the end wall boundary layers and secondary flow was determined to be 0.018 at the design critical velocity ratio. Because the secondary flow losses for small aspect ratio vanes is generally a significant portion of the total loss, an attempt to isolate this portion of the loss is desirable. To accomplish this the loss produced by the end wall boundary layers was first theoretically determined. The boundary layer growth on the end walls was calculated using the inviscid pressure distributions along the mean blade-to-blade streamlines near the hub and tip walls. This is a reasonable assumption since it is representative of the end wall loss had no secondary flow occurred. Therefore, the difference between the experimentally determined end wall and secondary flow loss (0.018) and the idealized end wall boundary layer calculation would represent the loss caused by secondary flow.

The end wall boundary layer parameters were calculated using the computer program described in reference 10. The inviscid mean blade-to-blade streamline pressure distribution through the vane passage was obtained from the TSONIC computer program (ref. 7). The end wall aftermixed kinetic energy losses were then calculated using Stewart's method (ref. 11) and determined to be 0.007 at the design critical velocity ratio. The kinetic energy loss due to secondary flow is, therefore, estimated to be 0.011 (i.e., 0.018 - 0.007). Since the total vane loss is 0.040 (i.e., 1 - 0.960), the secondary flow loss represents about 28 percent of the total vane loss.

Besides causing an appreciable stator loss, the secondary flow may also produce rotor incidence losses due to the stator exit flow angle maldistribution (see fig. 12). To determine this effect, rotor incidence angles were calculated from the measured stator exit flow conditions and design wheel speed. These are shown in figure 15 as are the design incidence angles. The effect of incidence on the core rotor blade losses has been experimentally determined in reference 12. Using this data, any additional incidence loss caused by the secondary flow over that which would occur for the design incidence angles was determined to be negligible. However, the effect of the stator secondary flow on the rotor secondary flow losses is not known.

The decrease in stator performance caused by secondary flow is likely to have a significant effect on turbine stage performance. Therefore, methods for reducing secondary flow effects are particularly important for small aspect ratio core turbines. A

number of techniques for reducing secondary flows have been reported in the literature. Some of these include blade twist (ref. 13), end wall contouring (ref. 14), and boundary layer fences on the vanes and end walls (ref. 9). For cooled stators it may also be possible to use the injected coolant to modify the secondary flow patterns.

SUMMARY OF RESULTS

The aerodynamic performance of a solid (uncooled) version of a core engine cooled stator vane was experimentally determined in a full-annular cascade, where three-dimensional effects could be obtained. The vanes were tested over a pressure ratio range that corresponds to mean-radius ideal aftermixed critical velocity ratios of 0.57 to 0.90. The design value for the vane is 0.778. Vane surface static-pressure distributions were measured and corresponding critical velocity ratios were compared with theoretical results. The variation in vane efficiency and aftermixed flow conditions with circumferential and radial position were obtained and compared with design values. Overall vane aftermixed efficiencies were obtained over this critical velocity ratio range and compared with results obtained in a two-dimensional cascade. The results of the investigation are summarized as follows:

1. The experimental vane surface critical velocity ratio distribution agreed well with the theoretical calculations obtained from the computer program TSONIC.

2. Efficiency contour plots at the vane exit survey plane indicated two vortex cores of high loss concentration (minimum efficiencies of about 0.72) located at the corners formed by the end walls and the suction surface of the vanes. These loss regions are associated with the secondary flows which are formed when the end wall boundary layers are deflected, from pressure to suction surface, in passing through the vane passage.

3. The aftermixed flow angles were found to be underturned in the vortex core regions by about 2° to 4°. Minimum aftermixed efficiencies of 0.939 and 0.944 were obtained for the hub and tip vortexes, respectively.

4. The overall aftermixed efficiency and the aftermixed efficiency at the mean radius for design critical velocity ratio are 0.960 and 0.978, respectively, and vary only slightly with aftermixed critical velocity ratio over the range investigated.

5. The losses due to end wall boundary layers and secondary flow was experimentally determined to be 0.018 at design critical velocity ratio. Of this loss, it was analytically determined that the end wall boundary layer loss was 0.007 and, therefore, the loss due to secondary flow is 0.011 for this vane.

Lewis Research Center,
National Aeronautics and Space Administration,
Cleveland, Ohio, January 30, 1975,
505-04.

REFERENCES

1. Szanca, Edward M.; Schum, Harold J.; and Hotz, Glen M.: Research Turbine for High-Temperature Core Engine Application. I - Cold-Air Overall Performance of Solid Scaled Turbine. NASA TN D-7557, 1974.

2. Stabe, Roy G.; and Kline, John F.: Aerodynamic Performance of a Core-Engine Turbine Stator Vane Tested in a Two-Dimensional Cascade of 10 Vanes and in a Single-Vane Tunnel. NASA TM X-2766, 1973.

3. Krause, Lloyd N.; and Gettelman, Clarence C.: Considerations Entering into the Selection of Probes for Pressure Measurements in Jet Engines. I. S. A. Proceedings. vol. 7, 1952, pp. 134-137.

4. Dudzinski, Thomas J.; and Krause, Lloyd N.: Flow-Direction Measurement with Fixed-Position Probes. NASA TM X-1904, 1969.

5. Goldman, Louis J.; and McLallin, Kerry L.: Cold-Air Annular-Cascade Investigation of Aerodynamic Performance of Cooled Turbine Vanes. I - Facility Description and Base (Solid) Vane Performance. NASA TM X-3006, 1974.

6. Katsanis, Theodore: FORTRAN Program for Quasi-Three-Dimensional Calculation of Surface Velocities and Choking Flow for Turbomachine Blade Rows. NASA TN D-6177, 1971.

7. Katsanis, Theodore: FORTRAN Program for Calculating Transonic Velocities on a Blade-to-Blade Stream Surface of a Turbomachine. NASA TN D-5427, 1969.

8. Rohlik, Harold E.; Kofskey, Milton G.; Allen, Hubert W.; and Herzig, Howard Z.: Secondary Flows and Boundary-Layer Accumulations in Turbine Nozzles. NACA Rep. 1168, 1954.

9. Prümper, H.: Application of Boundary Layer Fences in Turbomachinery. Boundary Layer Effects in Turbomachines, J. Surdigue, ed., AGARD-AG-164, Advisory Group for Aerospace Research & Development, Paris (France), 1972, pp. 311-331.

10. McNally, William D.: FORTRAN Program for Calculating Compressible Laminar and Turbulent Boundary Layers in Arbitrary Pressure Gradients. NASA TN D-5681, 1970.

11. Stewart, Warner L.: Analysis of Two-Dimensional Compressible-Flow Loss Characteristics Downstream of Turbomachine Blade Rows in Terms of Basic Boundary-Layer Characteristics. NACA TN 3515, 1955.

12. Stabe, Roy G.; and Kline, John F.: Incidence Loss for a Core Turbine Rotor Blade in a Two-Dimensional Cascade. NASA TM X-3047, 1974.

13. Ehrich, F. F.: Secondary Flows in Cascades of Twisted Blades. J. Aeronautical Sciences, vol. 22, no. 1, Jan. 1955, pp. 51-60.

14. Burrows, LeRoy T.: Investigation of Factors Affecting Small Turbine Efficiency and Loss Prediction. USAAVLABS TR-69-54, Army Aviation Materiel Lab. (AD-859273), 1969.

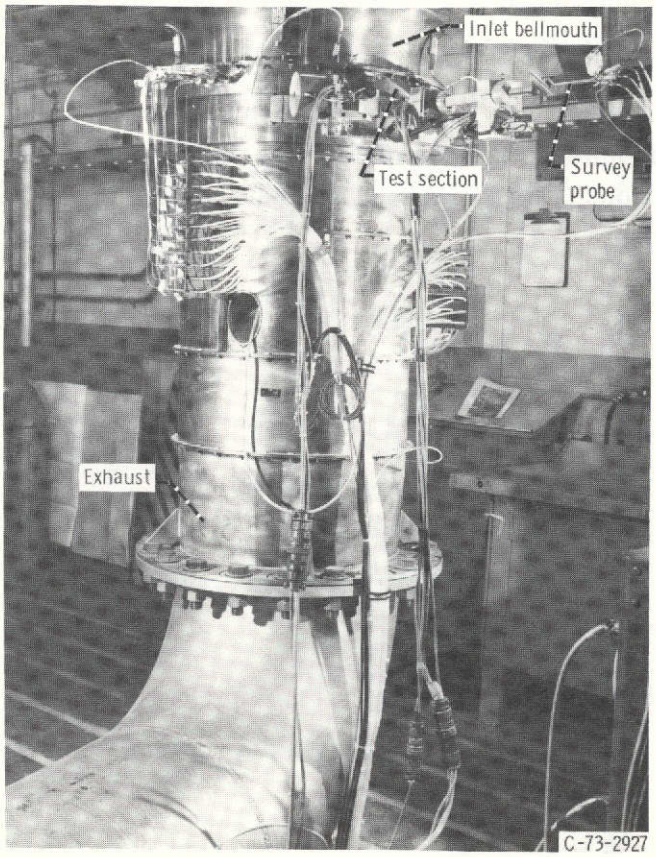

Figure 1. - Core stator annular cascade.

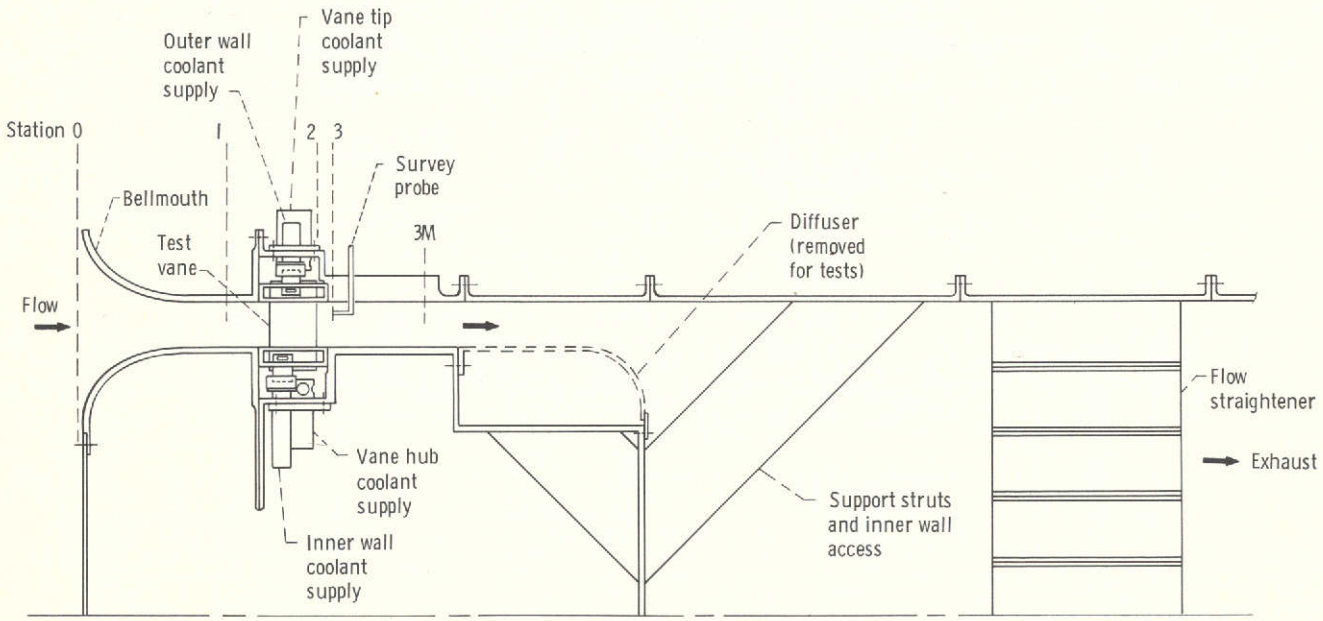

Figure 2. - Schematic cross-sectional view of core turbine stator cascade.

X		Y_L		Y_U	
cm	in.	cm	in.	cm	in.
0	0	0.508	0.200	0.508	0.200
0.127	0.050	-----	-----	.851	.335
.254	.100	-----	-----	1.003	.395
.381	.150	-----	-----	1.120	.441
.508	.200	-----	-----	1.212	.477
.635	.250	-----	-----	1.285	.506
.762	.300	.061	.024	1.341	.528
.889	.350	.117	.046	1.389	.547
1.016	.400	.163	.064	1.425	.561
1.143	.450	.201	.079	1.448	.570
1.270	.500	.236	.093	1.463	.576
1.397	.550	.267	.105	1.471	.579
1.524	.600	.292	.115	1.476	.581
1.778	.700	.328	.129	1.461	.575
2.032	.800	.358	.141	1.427	.562
2.286	.900	.376	.148	1.377	.542
2.540	1.000	.384	.151	1.321	.520
2.794	1.100	.381	.150	1.255	.494
3.048	1.200	.368	.145	1.191	.469
3.302	1.300	.353	.139	1.110	.437
3.556	1.400	.328	.129	1.026	.404
3.810	1.500	.297	.117	.942	.371
4.064	1.600	.262	.103	.848	.334
4.318	1.700	.221	.087	.747	.294
4.572	1.800	.178	.070	.635	.250
4.826	1.900	.130	.051	.521	.205
5.080	2.000	.084	.033	.399	.157
5.334	2.100	.025	.010	.267	.105
5.552	2.186	.089	.035	.089	.035

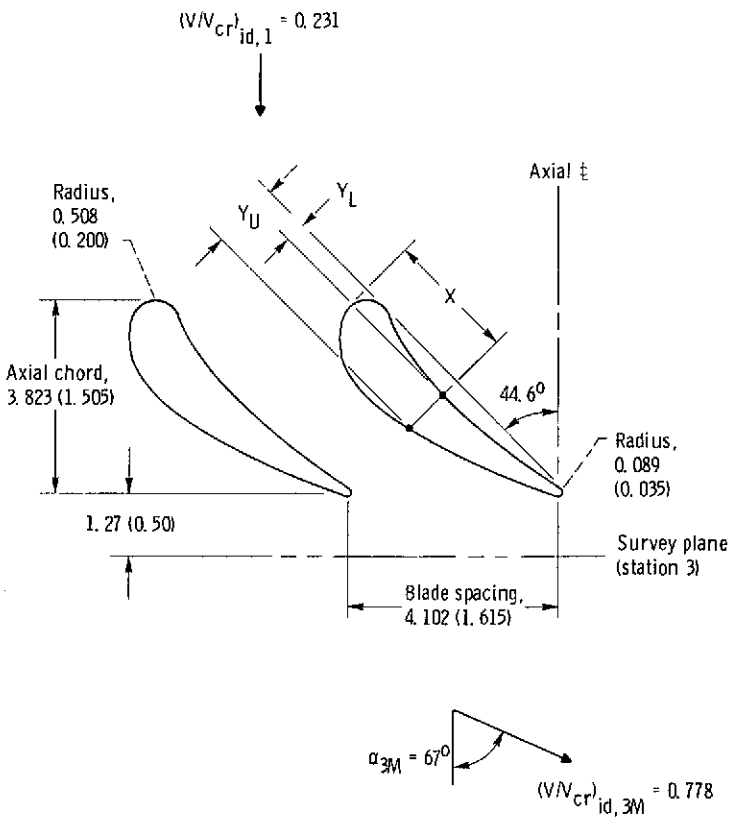

Figure 3. - Core turbine stator vane geometry at mean section. (All dimensions in cm (in.) except as noted.)

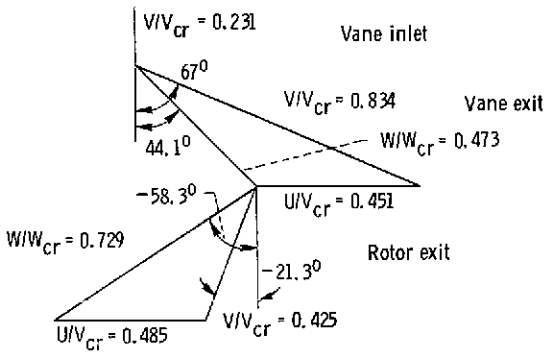

(a) Hub section.

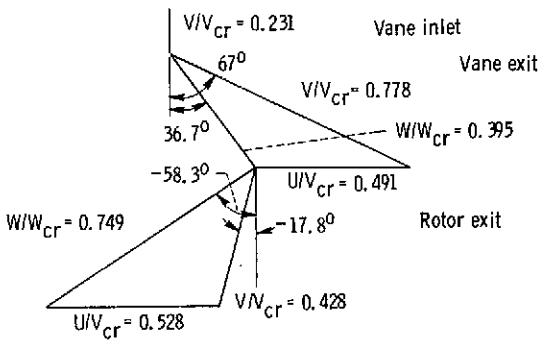

(b) Mean section.

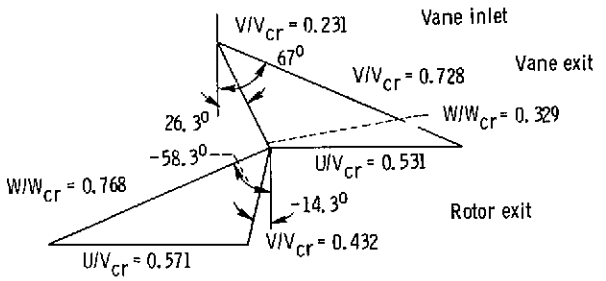

(c) Tip section.

Figure 4. - Turbine design velocity diagram.

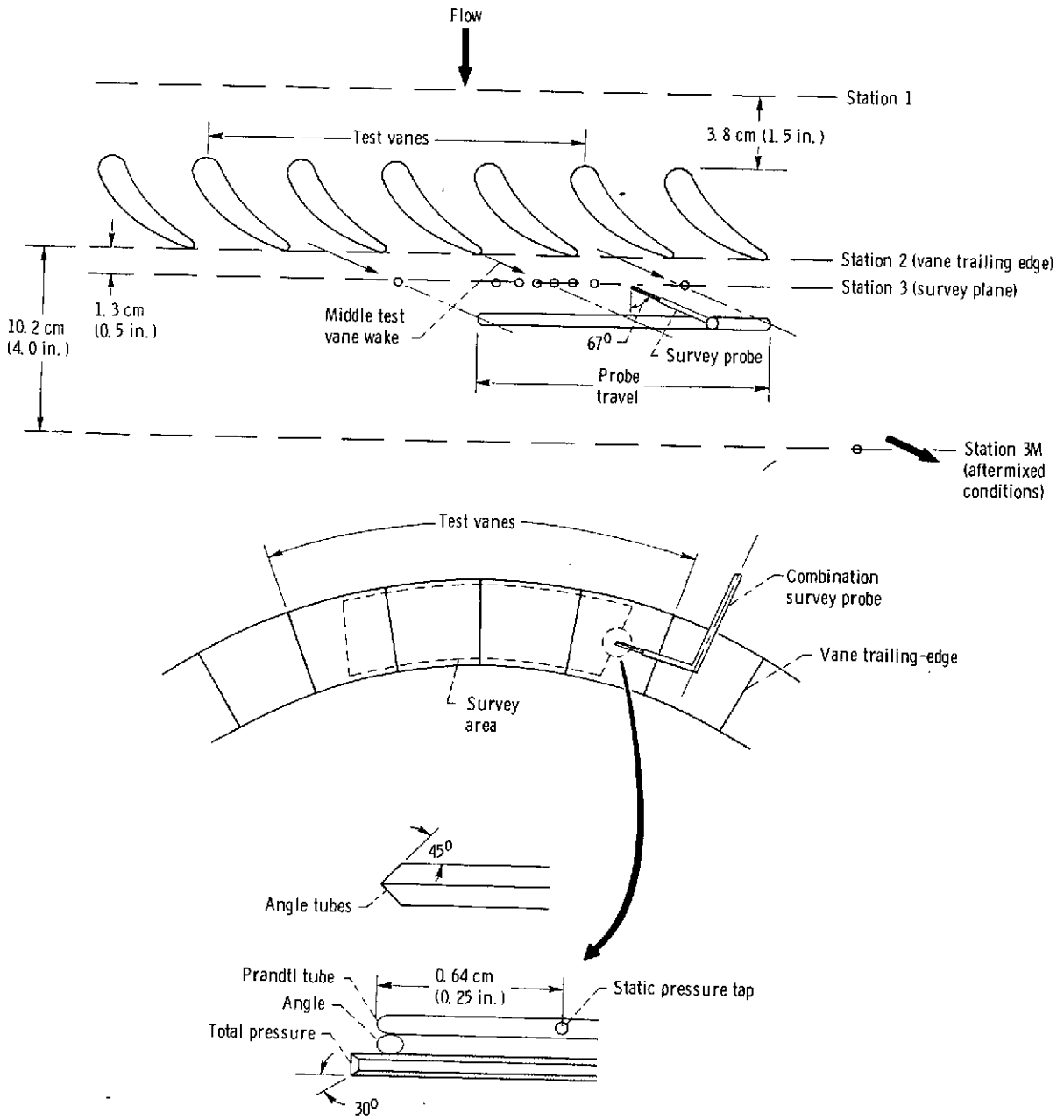

Figure 5. - Schematic of instrumentation for survey data.

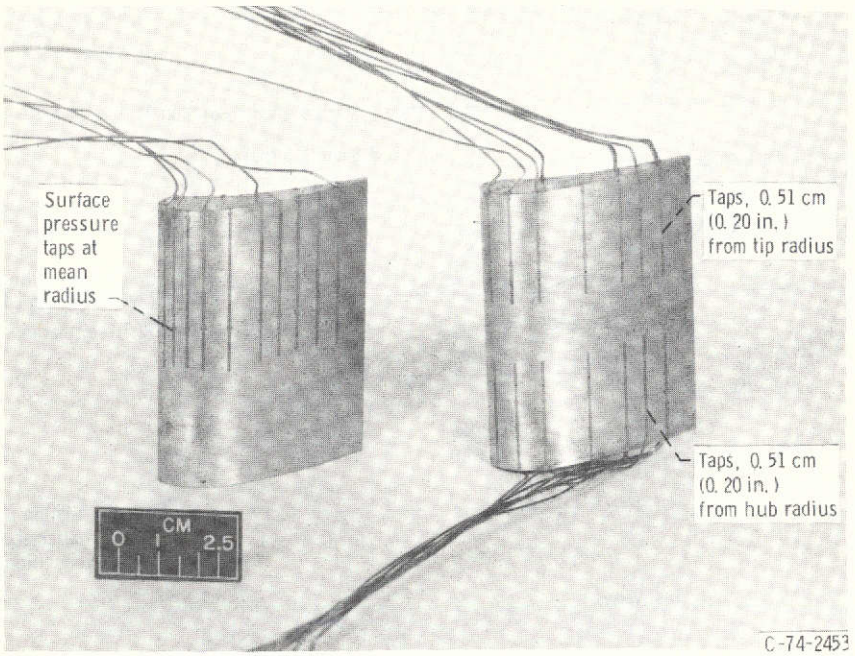

Figure 6. - Instrumented solid vanes.

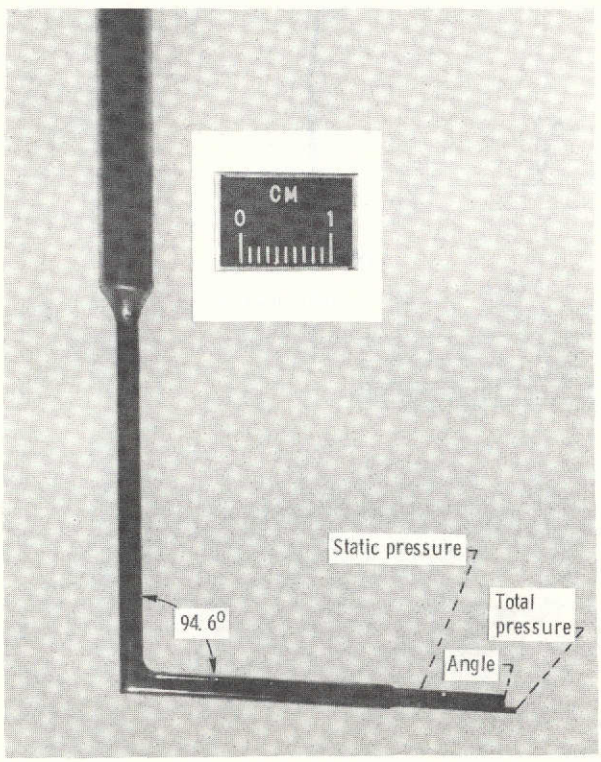

Figure 7. - Combination survey probe.

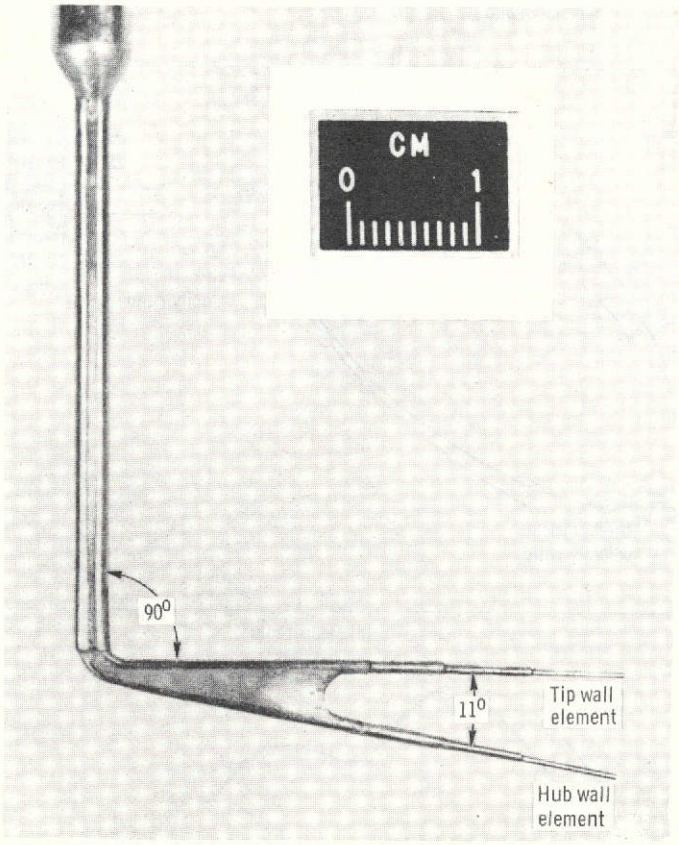

Figure 8. - End wall total pressure probe.

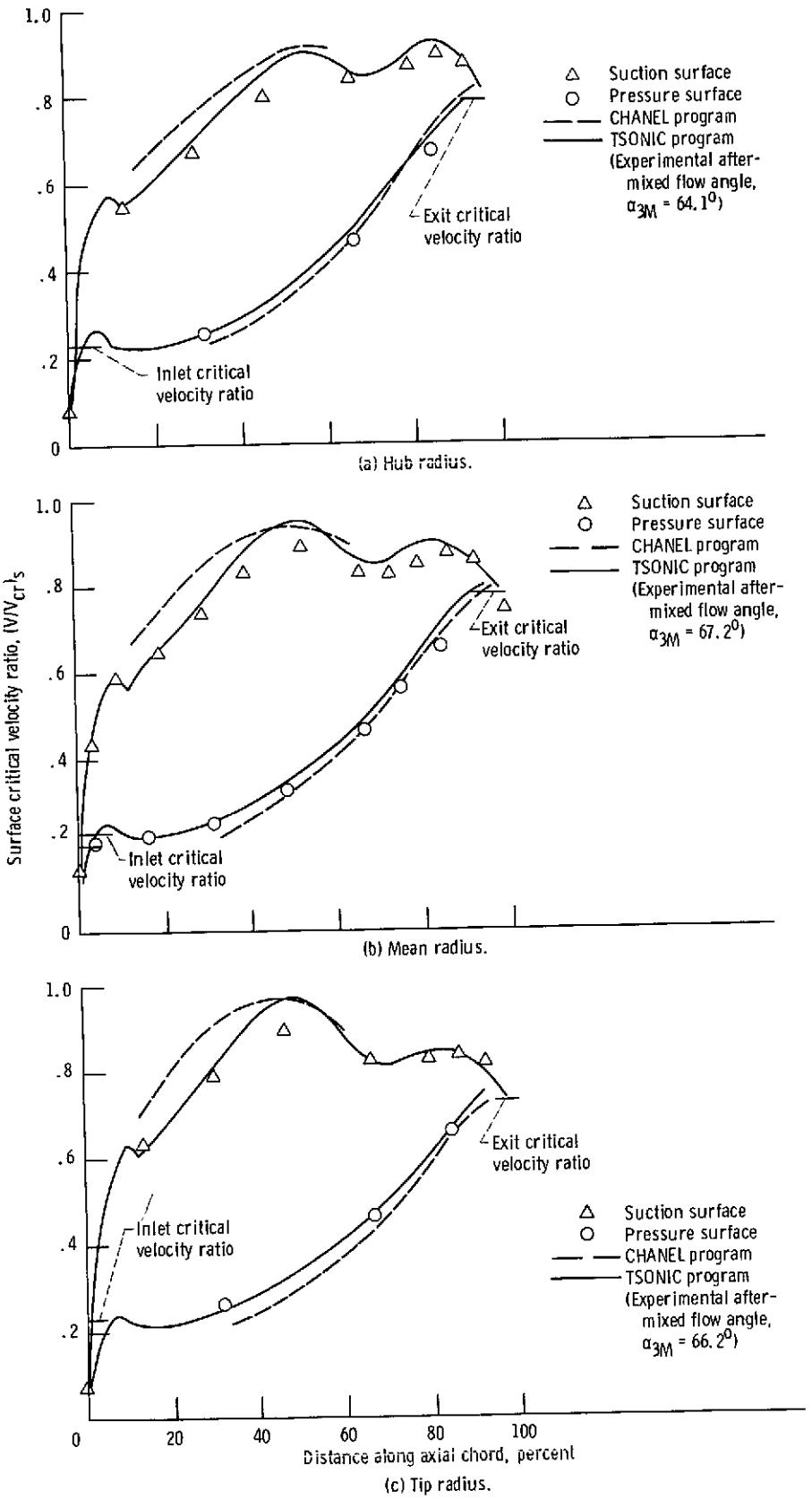

Figure 9. - Distribution of vane surface critical velocity ratio at ideal aftermixed critical velocity ratio of 0.785.

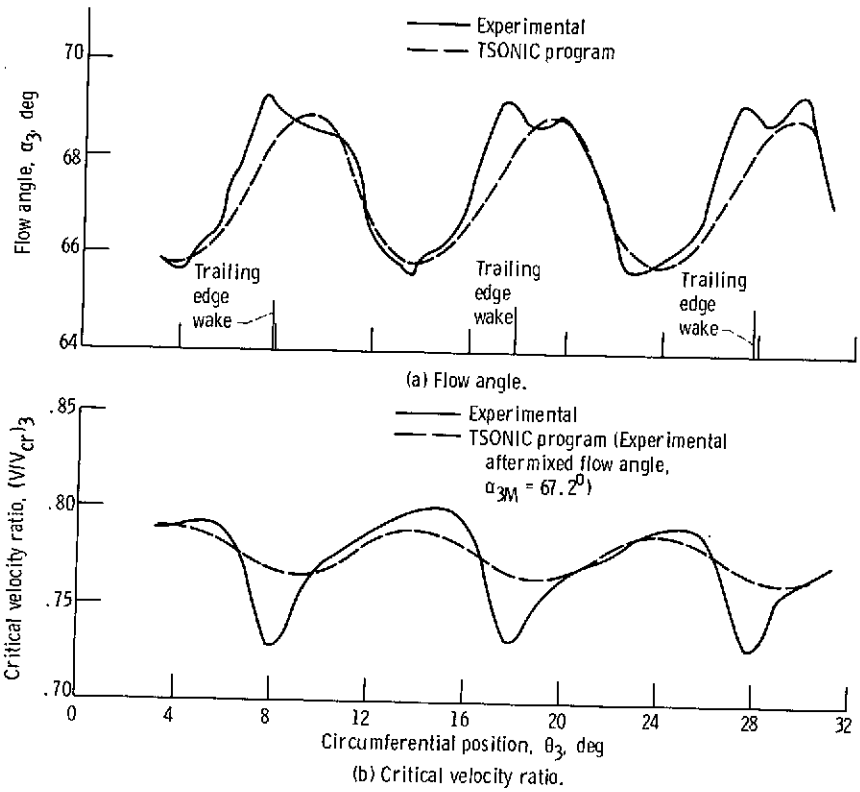

Figure 10. - Comparison of experimental and theoretical circumferential variation of exit flow angle and critical velocity ratio at mean radius and ideal aftermixed critical velocity ratio of 0.785.

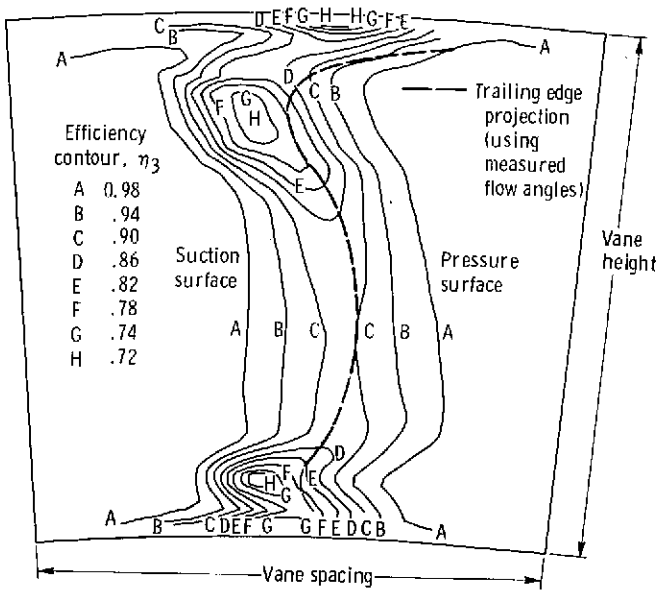

Figure 11. - Contours of efficiency at survey plane at ideal aftermixed critical velocity of 0.785.

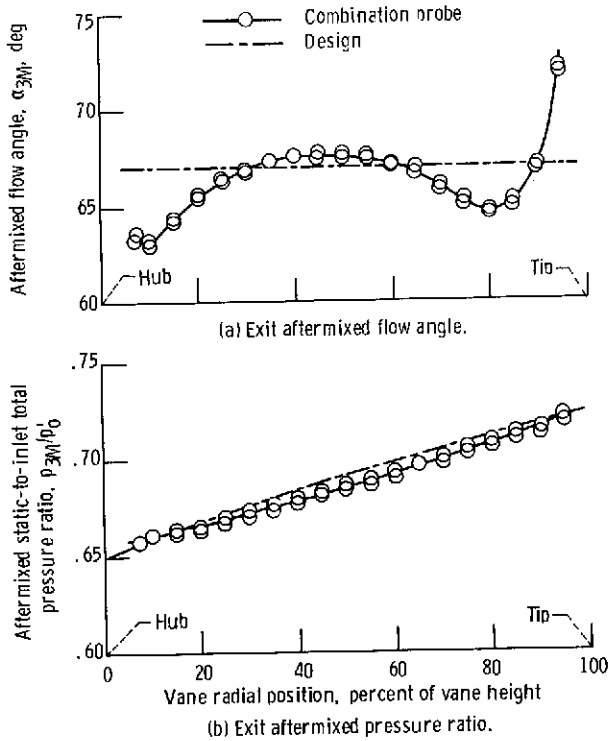

Figure 12. - Variation of aftermixed flow angle and static-to-total pressure ratio with radial position at ideal aftermixed critical velocity ratio of 0.785.

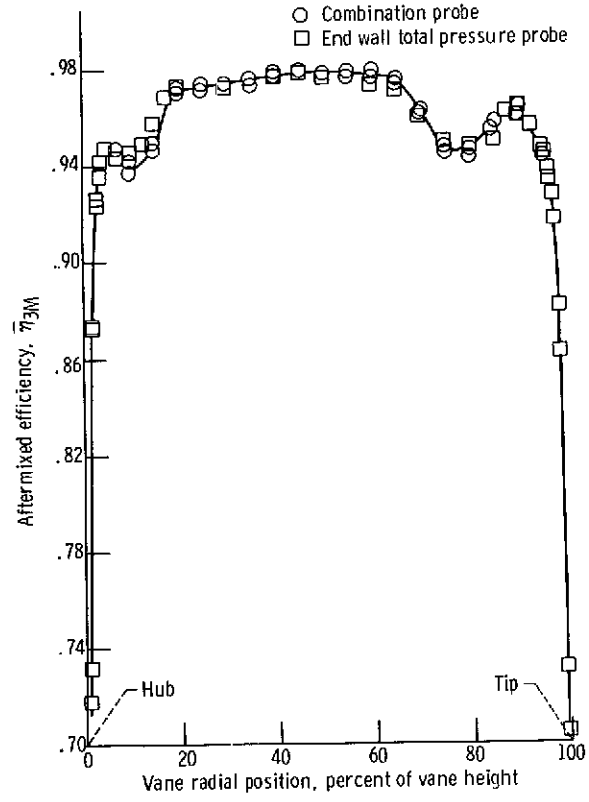

Figure 13. - Variation of aftermixed efficiency with radial position at ideal aftermixed critical velocity ratio of 0.785.

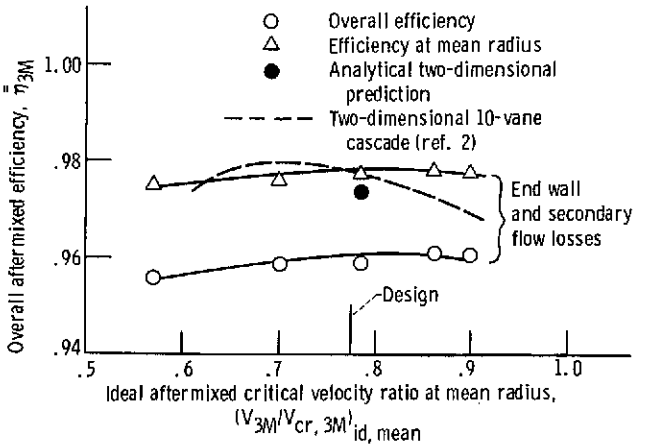

Figure 14. - Overall aftermixed efficiency as function of ideal aftermixed critical velocity ratio.

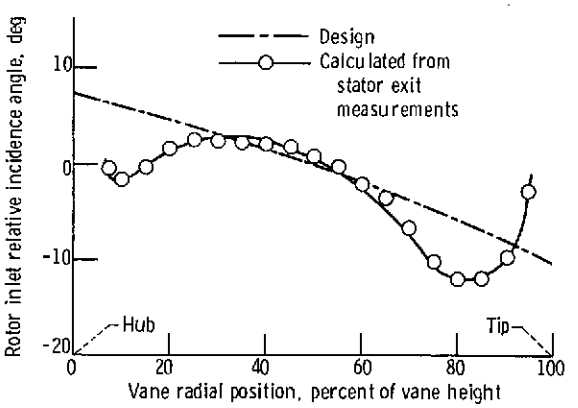

Figure 15. - Variation of rotor inlet relative incidence angle with radial position at ideal aftermixed critical velocity ratio of 0.785.